ORIGINAL ARTICLE

Autoclustering of Non-small Cell Lung Carcinoma Subtypes on ^{18}F-FDG PET Using Texture Analysis: A Preliminary Result

**Seunggyun Ha · Hongyoon Choi · Gi Jeong Cheon ·
Keon Wook Kang · June-Key Chung ·
Euishin Edmund Kim · Dong Soo Lee**

Abstract

Purpose Texture analysis on ^{18}F-fluorodeoxyglucose positron emission tomography (^{18}F-FDG PET) scan is a relatively new imaging analysis tool to evaluate metabolic heterogeneity. We analyzed the difference in textural characteristics between non-small cell lung carcinoma (NSCLC) subtypes, namely adenocarcinoma (ADC) and squamous cell carcinoma (SqCC).

Methods Diagnostic ^{18}F-FDG PET/computed tomography (CT) scans of 30y patients (median age, 67; range, 42-88) with NSCLC (17 ADC and 13 SqCC) were retrospectively analyzed. Regions of interest were manually determined on selected transverse image containing the highest SUV value in tumors. Texture parameters were extracted by *histogram-based algorithms*, *absolute gradient-based algorithms*, *run-length matrix-based algorithms*, *co-occurrence matrix-based algorithms*, and *autoregressive model-based algorithms*. Twenty-four out of hundreds of texture features were selected by three algorithms: *Fisher coefficient, minimization of both classification error probability and average correlation*, and *mutual information*. Automated clustering of tumors was based on the most discriminating feature calculated by linear discriminant analysis (LDA). Each tumor subtype was determined by histopathologic examination after biopsy and surgery.

Results Fifteen texture features had significant different values between ADC and SqCC. LDA with 24 automate-selected texture features accurately clustered between ADC and SqCC with 0.90 linear separability. There was no high correlation between SUV$_{max}$ and texture parameters ($|r| \leq 0.62$).

Conclusion Each subtype of NSCLC tumor has different metabolic heterogeneity. The results of this study support the potential of textural parameters on FDG PET as an imaging biomarker.

Keywords Positron emission tomography · F-18 Fluorodeoxyglucose · Carcinoma · Non-small cell lung · Texture analysis · Cluster analysis

S. Ha · H. Choi · G. J. Cheon · K. W. Kang · J.-K. Chung · D. S. Lee
Department of Nuclear Medicine, Seoul National University
Hospital, Seoul, Korea

S. Ha · H. Choi · E. E. Kim · D. S. Lee
Department of Molecular Medicine and Biopharmaceutical Sciences,
Graduate School of Convergence Science and Technology, and
College of Medicine or College of Pharmacy, Seoul National
University, Seoul, Korea

G. J. Cheon · K. W. Kang · J.-K. Chung
Cancer Research Institute, Seoul National University, Seoul, Korea

E. E. Kim
Department of Radiological Science, University of California at
Irvine, Irvine, CA, USA

G. J. Cheon (✉)
Department of Nuclear Medicine, Seoul National University College
of Medicine, 101 Daehak-RoJongno-Gu Seoul 110-744, Korea
e-mail: larrycheon@gmail.com

Introduction

In Korea as well as USA, lung cancer is the most common cause of cancer-related deaths [1]. The conventional treatment strategy in advanced lung cancer was determined based on the simplified cancer type classification, namely, non-small cell lung carcinoma (NSCLC) and small cell carcinoma (SCLC), although NSCLC is a heterogeneous disease group including adenocarcinoma (ADC) and squamous cell carcinoma (SqCC). Recent advances in targeted anti-lung cancer agents emphasize certain subclassifications of tumor type in NSCLC, especially in ADC.

Histopathologic examination is a "gold standard" in tumor subclassification; however, these approach occasionally

provide failed results due to inadequate tissue sample [2]. Noninvasive metabolic imaging of tumors may have complementary roles to histopathologic evaluation. Prior studies have shown the relationship between SUV_{max} of ^{18}F-fluorodeoxyglucose positron emission tomography (^{18}F-FDG PET) scan and histopathologic diagnosis [3]. Likewise, divergence of imaging analysis methods may lead to improved knowledge of tumor characterization [4, 5].

The digital PET image is composed of voxels and each one has a value in the gray-level intensity of the volume element in space [6]. The gray-level intensity is a representative value of glucose metabolism within the ^{18}F-FDG PET image, so gross texture of a lesion within the image may represent its histopathologic characteristics. Texture analysis is a mathematical pattern analysis technique and it quantifies the inter-relationships of the pixels or voxels via complex and variable mathematical methods [4]. Although the human eye is a good tool for discriminating the texture characteristics of a lesion, it has disadvantages, including being hard to achieve objectification. In addition, the visual system is able to recognize limited patterns of the texture. So the texture analysis based on a mathematical approach is a promising tool for recognizing hidden patterns of lesion for classification.

We hypothesized that metabolic heterogeneity reflects the histopathologic characteristics of a tumor, and by extension, molecular marker expression. This study is a preliminary study before evaluating the potential of metabolic heterogeneity as a predictive marker, so we analyzed the correlation between metabolic heterogeneity and histopathologic characteristics.

## Materials and Methods

Subjects and ^{18}FDG-PET/CT Imaging

Thirty patients with NSCLC as ADC and SqCC, who had received a basal ^{18}F-FDG PET/computed tomography (CT) during January to December of 2012, were included in this analysis. Pathologic confirmation of tumor was done by percutaneous needle aspiration (PCNA) and/or surgical resection. All the patients had been more than 6 h of fasting time before ^{18}F-FDG PET/CT scan. Fasting BST were regulated as less than 120. Each of the patients was injected with 5.18 MBq/kg of ^{18}F-FDG intravenously. Sixty minutes after injection, torso PET/CT scans were obtained on a Biograph 40 scanner (Siemens Medical Solutions, Knoxvillle, TN). Matrix size was 200 × 200 and voxel size was 2.6×2.6× 2.5 mm^3. PET image reconstruction was subsequently performed with ordered subsets-expectation maximization algorithm.

Texture Image Analysis

After the PET scan was obtained, texture feature extraction was processed as follows. Firstly, tumor on PET scan was segmented by drawn region of interest (ROI). We chose a transverse slice of each PET scan, which contained the highest SUV value in the tumor. And then, a representative two-dimensional (2D) ROI containing the visible tumor with the highest SUV value was manually drawn for each patient. Secondly, voxel-intensity was resampled with 64 gray levels and normalized to the mean±3 standard deviations (SD) for minimizing the error affected by contrast and brightness variation [7]. The final step was texture feature extraction from segmented and normalized tumor ROI using different algorithms, such as *histogram-based*, *absolute gradient (Gr)-based*, *run-length matrix-based*, *co-occurrence matrix (COM)-based*, and *autoregressive model-based methods*. The overall steps are briefly summarized on Fig. 1. More than 200 texture parameters per each ROI were extracted in this study. *The histogram-based features* including mean, variance, skewness, and kurtosis were calculated. *The Gr-based parameters* were calculated for spatial gray-level variance. The *run-length matrix-based parameters* about linear gray-level uniformity were calculated at 0, 45, 90 and 135 degrees. *The COM-based parameters* were about different combinations of gray levels of pixels in an image. For example, they calculated how often a pixel of intensity i co-occurred to another pixel of intensity j with pre-defined relationship of certain distance and direction. We computed for 20 vectors with five distances and four angles—0, 45, 90 and 135 degrees—in this analysis. *The autoregressive model-based parameters* computed the spatial relationship among neighborhood pixels. The formulae of several texture parameters which had significance in our data or were needed to describe them are shown in the Table 1. The rest of the texture feature extraction formulae which were included in this analysis can be found in the manual [8]. We used the software MaZda v.4.6 & B11 (The Technical University of Lodz, Institute of Electronics, Poland) for ROI drawing, texture parameter acquisition and analysis.

Feature Selection and Tissue Classification

We used three feature reduction methods to determine ten features per each method with high distinguishing ability between ADC and SqCC, as following subsets in MaZda v.4.6 software: (1) the largest Fisher coefficient (F), a between-class variance to within-class variance ratio, (2) minimization of both classification error probability and average correlation (PA), and (3) mutual information (MI), dependence between random variables (Table 3). The definition and detailed formulae of these subsets can be found in the manual [8]. All of the automatically selected parameters after
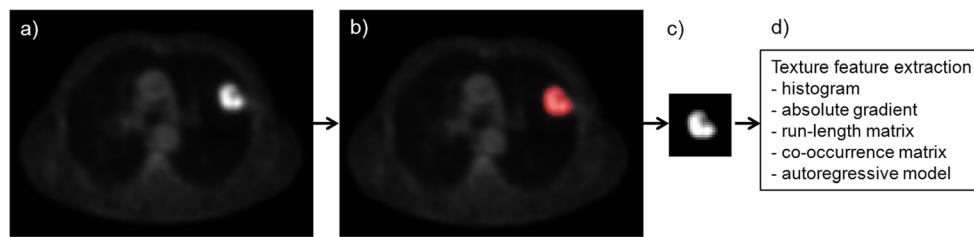
Fig. 1 Brief process of texture analysis on PET scan. First step is selection of the representative transverse image with highest SUV of tumor (**a**). Next, tumor is segmented by ROI with manual process (**b**). Segmented tumor is resampled by normalization with restriction of voxel intensity range (**c**). Final step is texture feature extraction by variable algorithms (**d**)

Table 1 Texture Parameters

Texture features	Formula or assumption
1. *Histogram-based features*	Assumption) $p(i)$ is a normalized histogram value for a pixel intensity I. μ is mean value.
Variance (σ^2)	$\sigma^2 = \sum\limits_{i=1}^{N} (i-\mu)^2 p(i)$
2. *Absolute gradient-based parameters*	Assumption) $x(i,j)$ is a pixel intensity at (i,j) position
Absolute gradient value [G(i,j)] for 5 × 5 matrix of M elements	$G(i,j) = \sqrt{\left(x_{i+2,j} - x_{i-2,j}\right)^2 + \left(x_{i,j+2} - x_{i,j-2}\right)^2}$
Mean of G(i,j), (GrMean)	$GrMean = \frac{1}{M} \sum\limits_{i,j \in ROI} G(i,j)$
Variance of G(i,j), (GrVariance)	$GrVariance = \frac{1}{M} \sum\limits_{i,j \in ROI} (G(i,j) - GrMean)^2$
Ratio of non-zero G(i,j) matrix elements, (GrNonZeros)	Ratio of non-zero G(i,j) values
3. *Run-length matrix-based parameters*[a]	
4. *Co-occurrence matrix-based parameters*	Assumption) $p(i,j)$ is the joint probability of co-occurring pixel intensity values i and j. N_x is a number of pixel intensities.
	$p_{x+y}(k) = \sum\limits_{i=1}^{N_x} \sum\limits_{j=1}^{N_x} p(i,j), \; i+j = k$
	$p_{x-y}(k) = \sum\limits_{i=1}^{N_x} \sum\limits_{j=1}^{N_x} p(i,j), |\cdots i-j\,| = k$
Angular second moment (AngScMom)	$AngScMom = \sum\limits_{i=1}^{N_x} \sum\limits_{j=1}^{N_x} p(i,j)^2$
Entropy	$Entropy = -\sum\limits_{i=1}^{N_x} \sum\limits_{j=1}^{N_x} p(i,j)\log(p(i,j))$
Inverse difference moment (InvDfMom)	$InvDfMom = \sum\limits_{i=1}^{N_x} \sum\limits_{j=1}^{N_x} \frac{1}{1+(i-j)^2} p(i,j)$
Sum of squares (SumOfSqs)	$SumOfSqs = \sum\limits_{i=1}^{N_x} \sum\limits_{j=1}^{N_x} (i-\mu_x)^2 p(i,j)$
Sum entropy (SumEntrp)	$SumEntrp = -\sum\limits_{i=1}^{2N_x} p_{x+y}(i)\log\left(p_{x+y}(i)\right)$
Sum average (SumAverg)	$SumAverg = \sum\limits_{i=1}^{2N_x} i\, p_{x+y}(i)$
Sum variance (SumVarnc)	$SumVarnc = \sum\limits_{i=1}^{2N_x} (i-SumAverg)^2 p_{x+y}(i)$
Difference entropy (DifEntrp)	$DifEntrp = -\sum\limits_{i=1}^{N_x} p_{x-y}(i)\log\left(p_{x-y}(i)\right)$
Difference variance (DifVarnc)	$DifVarnc = \sum\limits_{i=0}^{N_x-1} \left(i-\mu_{x-y}\right)^2 p_{x-y}(i)$
5. *Autoregressive model-based parameters* [a]	

[a] No texture feature with significant value in this study; cf. Table 3.

standardization were enrolled in linear discriminant analysis (LDA), which is a type of multivariate analysis for classification and dimension reduction [9]. The results of LDA were shown as the most discriminating features (MDF) and the nearest neighbor method ($k=1$) was used for the MDF.

Statistics

All the continuous data were written as mean±1 SD. The Mann-Whitney U-test was employed to make a comparison between means of selected texture features of ADC and SqCC, or male and female. Selected texture features were evaluated correlation with SUV_{max} and tumor size using the Pearson correlation coefficient (r). When $|r|$ was higher than 0.7, we regarded that there was strong correlation between two parameters. A p value of 0.05 was regarded as a threshold for a certain statistical significance. We used software SPSS v.18.0 (SPSS, Chicago, IL, USA) for statistic calculation. The usefulness of LDA results for clustering tumor was expressed as linear separability, which was calculated by B11 software. When linear separability changes from 0.0 to 1.0, the result becomes more separable.

Results

Patients

Of the 30 patients (median age, 67; range, 42-88) included, 16 patients were men and 14 patients were women. Overall, 17 ADCs and 13 SqCCs were involved in the analysis. On ^{18}F-FDG PET images, the mean diameter of ADC was 37.8±18.3 mm and that of SqCC was 49.9±14.1 mm. Summarized characters of the patients are presented in Table 2.

Comparison of Automatically Selected Texture PET Parameters Between ADC and SqCC

Six texture parameters selected by F, PA and MI texture feature selection subsets were overlapped, so that, overall, 24 parameters were included in this analysis. There were one gray-level histogram-based parameter (Variance), two *Gr-based parameters*, variance of absolute gradient (GrVariance) and ratio of non-zero absolute gradient values (GrNonZeros), and 21 *COM-based parameters*. There was no *run-length matrix-based parameter* or *autoregressive model-based parameter* in the automated parameter selection. Mann-Whitney U-test revealed that 16 quantitative PET parameters including SUV_{max} and 15 texture parameters, composed of *one Gr-based parameter* and 14 *COM-based parameters*, showed significant difference of mean values between ADC

Table 2 Patient Characteristics

Patient no.	Sex	Age (years)	Histopathology	Tumor size (mm)
1	M	78	ADC	41.9
2	M	69	ADC	50.1
3	M	71	ADC	92.3
4	F	76	ADC	39.8
5	F	52	ADC	25.8
6	M	46	ADC	20.8
7	F	61	ADC	19
8	F	63	ADC	21.8
9	F	74	ADC	36.5
10	F	64	ADC	25.1
11	F	52	ADC	22.8
12	M	59	ADC	52.9
13	F	75	ADC	44.6
14	F	73	ADC	21.3
15	F	74	ADC	37.1
16	F	42	ADC	30
17	F	59	ADC	60.5
18	M	76	SqCC	62.8
19	M	63	SqCC	69.7
20	M	88	SqCC	33.4
21	F	67	SqCC	31.7
22	M	67	SqCC	73.3
23	M	57	SqCC	54
24	M	73	SqCC	25.2
25	M	64	SqCC	49.7
26	M	70	SqCC	43.7
27	M	62	SqCC	49.1
28	M	79	SqCC	48.5
29	F	73	SqCC	63.3
30	M	59	SqCC	44.1

Tumor size measured by longest diameter of ROI from selected PET image slices

and SqCC (Table 3). SUV_{max} showed the most significant association to tumor pathology in these data ($p=0.001$).

Correlation Between Automatically Selected Texture PET Parameters and SUV_{max}

Fifteen of 24 automatically selected texture parameters have significant correlation to SUV_{max} ($p<0.05$, respectively). Range of calculated $|r|$ levels with significance in these parameters was 0.33–0.62. Among the texture parameters which have significant mean level difference between ADC and SqCC, there were 12 texture parameters with significant correlation to SUV_{max}. The results of simple correlation analysis were described in Table 4.

Table 3 PET Texture Parameter Analysis

PET parameters	Feature selection			Comparison of mean values between ADC and SqCC		
	Fisher	PA	MI	ADC	SqCC	p value
S(1,0) Entropy[a, c]	1.5999	-	0.3545	2.20±0.21	2.41±0.12	0.004*
S(1,0) SumEntrp[a, c]	1.4775	-	0.396	1.67±0.12	1.78±0.05	0.006*
S(0,1) Entropy[a, c]	1.4501	-	0.3308	2.18±0.21	2.38±0.11	0.008*
S(0,3) SumOfSqs[a, c]	1.3838	-	0.3335	113.47±10.31	102.25±9.26	0.004*
S(0,1) AngScMom[a, c]	1.3329	-	0.3185	0.0084±0.0036	0.0052±0.0012	0.017*
GrNonZeros[a]	1.3267	-	-	0.98±0.02	0.95±0.03	0.004*
S(1,0) AngScMom[a]	1.2776	-	-	0.0080±0.0037	0.0048±0.0013	0.006*
S(2,0) SumOfSqs[a]	1.2748	-	-	109.57±7.47	101.11±8.11	0.007*
S(1,-1) AngScMom[a]	1.269	-	-	0.0072±0.0033	0.0044±0.0013	0.007*
S(0,4) SumOfSqs[a]	1.2516	-	-	118.95±13.62	105.39±10.95	0.006*
S(4,0) DifEntrp[b]	-	0.4096	-	1.37±0.087	1.41±0.041	0.133
S(1,-1) SumOfSqs[b]	-	0.4487	-	107.40±4.93	101.78±5.58	0.006*
S(0,4) InvDfMom[b]	-	0.4528	-	0.074±0.023	0.096±0.030	0.039*
S(5,0) SumVarnc[b]	-	0.4569	-	157.33±67.81	181.17±39.16	0.245
S(5,5) SumOfSqs[b]	-	0.4651	0.3289	80.18±33.74	106.83±12.84	0.079
S(2,2) SumOfSqs[b]	-	0.477	-	113.30±11.39	102.92±8.52	0.01*
S(5,-5) InvDfMom[b]	-	0.4777	-	0.108±0.107	0.079±0.022	0.68
S(3,3) DifEntrp[b]	-	0.479	-	1.35±0.96	1.39±0.039	0.17
Variance[b]	-	0.4829	-	1,908,612±2,770,149	10,944,950±16,414,211	0.183
S(2,2) DifVarnc[b]	-	0.6	-	53.48±19.38	40.77±11.89	0.039*
S(5,0) DifEntrp[c]	-	-	0.4344	1.35±0.11	1.44±0.04	0.002*
S(0,3) DifVarnc[c]	-	-	0.3304	50.93±22.40	40.38±9.62	0.263
S(5,0) DifVarnc[c]	-	-	0.3225	96.99±36.74	82.57±15.73	0.432
GrVariance[c]	-	-	0.3205	1.43±0.49	1.65±0.73	0.432
SUV$_{max}$[d]				10.06±5.18	16.95±4.52	0.001*

* $p<0.05$, statically significant

[a, b, c] Parameters selected by Fisher coefficient, PA, and MI, respectively

[d] SUV$_{max}$ values were suggested for comparison with texture parameters

Relationship With Texture Features and Clinical Data

Each of 24 automatically selected texture features was compared with clinical data, including gender and tumor size. There was no texture feature which has significant difference of mean values according to patient gender ($p>0.05$, respectively, Table 4). Linear correlation analysis revealed that 19 of 24 texture features had significant correlation to tumor size (Table 4). Seven texture features had |r| values more than 0.7. Size itself did not have association to tumor pathologies ($p>0.05$).

Autoclustering by Linear Discriminant Analysis

Autoclustering by LDA with those 15 texture parameters which had significant difference between tumor subclassification calculated that MDF values as follows: ADC, -0.097± 0.071; SqCC, 0.127±0.096. Twenty-five of 30 lesions were

correctly clustered to their own tumor type (classification accuracy 83.33%). Two ADC and three SqCC lesions were misclassified. Linear separability was 0.64 (Fig. 2a). When analyzing with all the selected 24 parameters, each MDF value of ADC and SqCC, calculated by LDA, was -0.120± 0.044 and 0.157±0.049. LDA clustered lesions accurately according to their pathology between ADC and SqCC, with a classification accuracy of 100%. The linear separability of this autoclustering was 0.90 (Fig. 2b).

Discussion

^{18}F-FDG PET/CT scan is a well-established hybrid-functional imaging technique for cancer evaluation in the clinical field. ^{18}F-FDG PET scan enables non-invasive tumor evaluation for grading, staging and measuring the response to treatment with

Table 4 Comparison to Other Parameters

PET parameters	Correlation to SUV$_{max}$		Difference of texture features between genders			Correlation to Size	
	r	p value	Male	Female	p value	r	p value
S(1,0) Entropy	0.589	*0.001**	2.31±0.17	2.27±0.24	0.759	0.861	*<0.001**
S(1,0) SumEntrp	0.579	*0.001**	1.73±0.09	1.70±0.13	0.697	0.826	*<0.001**
S(0,1) Entropy	0.584	*0.001**	2.29±0.17	2.25±0.23	0.728	0.858	*<0.001**
S(0,3) SumOfSqs	-0.471	*0.009**	106.57±10.05	110.93±12.41	0.355	-0.655	*<0.001**
S(0,1) AngScMom	-0.585	*0.001**	0.006±0.002	0.008±0.004	0.473	-0.783	*<0.001**
GrNonZeros	-0.284	0.128	0.97±0.03	0.97±0.03	0.759	-0.748	*<0.001**
S(1,0) AngScMom	-0.622	*<0.001**	0.006±0.002	0.007±0.004	0.667	-0.741	*<0.001**
S(2,0) SumOfSqs	-0.504	*0.004**	104.65±7.62	107.34±9.95	0.355	-0.602	*<0.001**
S(1,-1) AngScMom	-0.529	*0.003**	0.006±0.002	0.006±0.004	0.580	-0.819	*<0.001**
S(0,4) SumOfSqs	-0.465	*0.010**	110.60±12.45	115.90±15.75	0.448	-0.683	*<0.001**
S(4,0) DifEntrp	0.386	*0.035**	1.39±0.05	1.39±0.10	0.728	0.302	0.105
S(1,-1) SumOfSqs	-0.397	*0.030**	0.006±0.002	0.007±0.004	0.120	-0.495	*0.005**
S(0,4) InvDfMom	0.252	0.179	104.65±7.62	107.34±9.95	0.423	0.394	*0.031**
S(5,0) SumVarnc	0.207	0.272	170.97±60.95	163.87±55.51	0.637	0.525	*0.003**
S(5,5) SumOfSqs	0.219	0.244	91.28±26.78	92.23±33.58	0.790	0.478	*0.008**
S(2,2) SumOfSqs	-0.380	*0.039**	105.95±10.05	112.06±12.24	0.154	-0.609	*<0.001**
S(5,-5) InvDfMom	-0.368	*0.046**	0.084±0.033	0.11±0.12	0.984	-0.325	0.080
S(3,3) DifEntrp	0.589	*0.001**	1.37±0.09	1.37±0.07	0.728	0.185	0.327
Variance	0.333	0.072	7.11±1.43	4.35±7.98	0.667	0.027	0.888
S(2,2) DifVarnc	-0.236	0.209	44.49±14.55	51.94±20.20	0.313	-0.636	*<0.001**
S(5,0) DifEntrp	0.542	*0.002**	1.38±0.07	1.39±0.12	0.667	0.611	*<0.001**
S(0,3) DifVarnc	-0.191	0.312	41.97±11.62	51.38±23.65	0.498	-0.574	*0.001**
S(5,0) DifVarnc	-0.246	0.190	87.35±25.46	94.61±35.06	0.667	-0.520	*0.003**
GrVariance	0.077	0.687	1.45±0.56	1.62±0.66	0.525	0.187	0.323
SUV$_{max}$			12.93±5.86	13.19±6.26	0.951	0.318	0.087

* $p<0.05$, statically significant

high sensitivity and specificity in certain cancers [10]. ^{18}F-FDG PET data allow a quantitative evaluation of glucose metabolism of tumor. Although a lot of previous studies have reported the clinical usefulness using SUV$_{max}$ and volumetric parameters, these conventional parameter-based analyses

have several limitations [4, 5, 11–13]. These parameters are classified into histogram-based parameters, so they also have the short-comings of histogram analysis. Histogram-based parameters cannot describe the gross texture coming from relationships of two or more voxels. For example, SUV$_{max}$
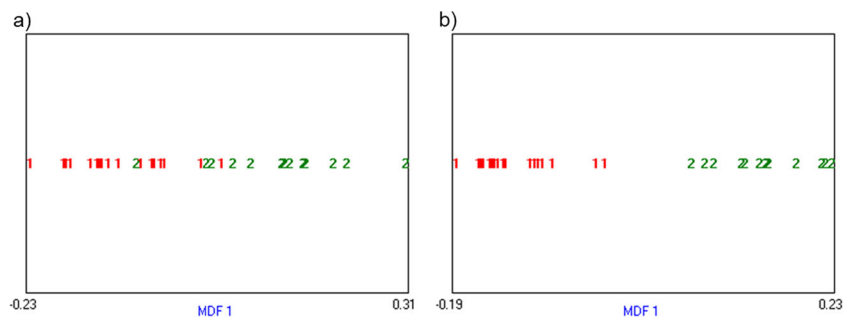
Fig. 2 Clustering analysis with PET texture features. LDA with 15 selected texture features which had significant association with tumor subtypes showed 0.64 of linear separability. There were 5 of 30 misclassified lesions (**a**). LDA with 24 selected texture features showed accurate discrimination between ADC and SqCC without misclassification. The linear separability of LDA is 0.90 (**b**). MDF 1 is the most discriminating feature presented by LDA. In these figures, ADC was marked as '1', and SqCC was marked as '2'

only reflects the highest value of metabolic activity in a tumor, and volumetric parameters such as metabolic tumor volume only reflect overall tumor burden.

Histopathological characteristics of tumor may compose the gross texture of the tumor not only on the tissue, but also on the images. Previous researches have investigated the potential of texture analysis in anatomical imaging such as US, CT and MRI, and presented the data supporting the hypothesis that texture features on images can discriminate the tissue types [14–16]. Regardless of these successes of texture analysis in anatomical imaging, developments in PET image analysis have been delayed because of its relatively poorer spatial resolution than that of anatomical images. To date, there have been only a few studies investigating the PET texture analysis, and these studies have been localized to prediction of prognosis and evaluation for radiotherapy planning [15]. However, these studies have some ambiguous points about the relationship between textural features and histopathologic characteristics of tumors [17].

Personalized medicine have become the issue of this era since targeted drugs proved clinical impact with survival prolongation, especially in NSCLC [18]. Image-mediated tumor characterization has potentials as non-invasive biomarker evaluation. Several previous PET quantitative analysis showed correlation of value of SUV_{max} and histopathological features including tumor subtypes, Ki-67 expression, EGFR mutation and Alk rearrangement [19, 20]. However, there are also some studies showing negative data to the relationship between SUV_{max} and tumor subtypes or EGFR expression in lung cancer [21].

Metabolic heterogeneity is a remarkable feature of malignancy, and the texture analysis provides quantifying analysis tools for evaluating tumor heterogeneity [22]. In our study, 15 extracted raw texture parameters of ^{18}F-FDG PET were significantly associated with histological subtypes of NSCLC in univariate analysis. Especially, 14 of the 15 texture parameters which had significant different values between ADC and SqCC were *COM-based texture parameters*. This is well consistent with previous studies by texture analysis on MRI and CT scans, which reported that the *COM-based texture parameter* looks like most valuable parameter for tissue characterization [14, 23]. *COM-based texture parameter* is a kind of second order texture feature which describes neighborhood gray-tone difference, and was generally interpreted to reflect the metabolic heterogeneity of entropy, energy, and contrast of tumor, so that these *COM-based texture parameters* have high association with tumor pathology stands to reason [17, 24].

There has been reported clinical usefulness of PET texture analysis in recent years. However, clinical application of PET texture parameter is still controversial. One of these concerns is about the unclear point of relationship to conventional parameters such as SUV_{max}. Furthermore, the analysis results that the most associated PET parameter to tumor pathology

was SUV_{max}, not selected PET texture parameters, further amplifies suspicion of the clinical usefulness of PET texture parameters. For the solution, we evaluated linear correlation between selected texture parameters and SUV_{max} to figure out their relationships. In this study, although 15 of 24 texture parameters were significantly correlated to SUV_{max}, there was no highly correlated texture parameter with SUV_{max} ($|r| \leq 0.62$). These results supported the validity of texture features in PET data analysis, which had distinct value to SUV_{max}. Additionally, we investigated the relationship of extracted texture features to clinical data in order to figure out the texture feature characteristics which were used in this study. Genders did not have any relationship to extracted texture features. On the other hand, many of extracted texture features showed significant correlations to tumor size. Besides, seven texture features had strong linear correlations to tumor size. Correlation of texture features to tumor size should be considered for tumor characterization by texture analysis. In this study, we did not use multivariate analysis including tumor size for tumor characterization, because tumor size itself did not have association to tumor histopathological feature in our data.

Actually, a single texture parameter is not enough to represent the gross texture of tumor. In regard to gross texture, the metabolic heterogeneity of tumor was composed of multiple texture patterns. In view of this, a complex of integrated different texture parameters is needed to describe the gross texture of a tumor. The LDA, feature extraction method for pattern recognition, was employed on PET texture features to develop an autoclustering of tumor as ADC and SqCC [25]. LDA with extracted texture parameters of ^{18}F-FDG PET using automate-subsets of F, PA and MI clustered subtypes of NSCLC with high accuracy. The clustering analysis outcomes especially showed that the more texture parameters were involved, the higher accuracy of clustering was obtained. LDA with 24 texture features did not show misclassification of tumor subtypes, although LDA with 15 texture features misclassified 5 of 30 tumors. These results strongly supported usefulness of PET texture feature complex for discrimination of tumor subtypes.

Further study can be considered in the aspect of discrimination between lung cancer and inflammation using texture analysis. This issue is clinically very important because these two pathologic events show increased FDG uptake which can mimic each other. However, the mechanisms of increased FDG uptake were different. Tumor cells have characteristic up-regulated altered glucose metabolism themselves, however, in the inflammatory lesion, increased FDG uptake is a result of the infiltration of activated inflammatory cells [26]. It is clinically not easy to distinguish between those two lesions based on FDG uptake on PET scan [27]. However, the assumption that those two different lesions, which have discriminating histopathologic features, show different

metabolic heterogeneity is reasonable. Although a previous study using texture analysis with *COM-based parameters* on CT scan has reported data for assessing the possibility for discrimination of tumor and inflammation, to our knowledge there were no reported data using PET texture analysis [23]. We also convince that application of texture analysis with clustering method to PET scan may be helpful to this clinical issue.

Our study has several limitations. In our retrospective study, we did not try to correct the partial volume effect. However, we studied tumors with greater than 1 cm in size, so that a partial volume effect may not significantly affect the results of our study. Another weakness is manually drawn tumor ROI for analysis. Automated drawing ROI methods may reduce intra- and inter-observer variation. Likewise, Galavis et al. [28] reported that some texture parameters exhibited large variations when PET images are acquired and processed with different modes. We included PET scans acquired on a single PET/CT system not to make factors of feature variability. However, this approach may restrict versatile application of the results of our research to other institutions which have different image acquisition and reconstruction systems for PET scans. Thus, the results obtained from texture feature analysis should be carefully interpreted in consideration of the PET imaging system.

Conclusions

Different subtypes of NSCLC, namely ADC and SqCC, have different characteristics of metabolic heterogeneity in our study. This preliminary study based on texture analysis and histopathological characteristics supports the potential of metabolic heterogeneity as an imaging biomarker for NSCLC. Texture analysis on metabolic images may help the advance of image-based personalized medicine.

Conflict of Interest   Seunggyun Ha, Hongyoon Choi, Gi Jeong Cheon, Keon Wook Kang, June-Key Chung, Euishin Edmund Kim and Dong Soo Lee declare no conflict of interest.

Informed Consent   This retrospective study was approved by the institutional review board in our institution in accordance with the ethical standards and with the Helsinki Declaration of 1975, as revised in 2000. The informed consent was waived under exemption.

References

1. Jung K-W, Park S, Kong H-J, Won Y-J, Lee JY, Seo HG, et al. Cancer statistics in Korea: incidence, mortality, survival, and prevalence in 2009. Cancer Res Treat. 2012;44(1):11–24.

2. Podbielski FJ, Rodriguez HE, Brown AM, Blecha MJ, Salazar MR, Connolly MM. Percutaneous biopsy in evaluation of lung nodules. JSLS. 2004;8(3):213–6.

3. Han B, Lin S, Yu L-J, Wang R-Z, Wang Y-Y. Correlation of 18F-FDG PET activity with expressions of survivin, Ki67, and CD34 in non-small-cell lung cancer. Nucl Med Commun. 2009;30(11):831–7.

4. Rahim MK, Kim SE, So H, Kim HJ, Cheon GJ, Lee ES, et al. Recent trends in PET image interpretations using volumetric and texture-based quantification methods in nuclear oncology. Nucl Med Mol Imaging. 2014:1-15.

5. Budiawan H, Cheon GJ, Im H-J, Lee SJ, Paeng JC, Kang KW, et al. Heterogeneity analysis of 18F-FDG uptake in differentiating between metastatic and inflammatory lymph nodes in adenocarcinoma of the lung: comparison with other parameters and its application in a clinical setting. Nucl Med Mol Imaging. 2013;47(4):232–41.

6. Castellano G, Bonilha L, Li LM, Cendes F. Texture analysis of medical images. Clin Radiol. 2004;59(12):1061–9.

7. Collewet G, Strzelecki M, Mariette F. Influence of MRI acquisition protocols and image intensity normalization methods on texture classification. Magn Reson Imaging. 2004;22(1):81–91.

8. Materka A. MaZda user's manual. Available at: http://www.eletel.p.lodz.pl/cost/progr_mazda_eng.html. 2002.

9. Balakrishnama S, Ganapathiraju A. Linear discriminant analysis—a brief tutorial. Institute for Signal and information Processing, Mississippi State University, Starkville. 1998.

10. Saif MW, Tzannou I, Makrilia N, Syrigos K. Role and cost effectiveness of PET/CT in management of patients with cancer. Yale J Biol Med. 2010;83(2):53.

11. Choi ES, Ha SG, Kim HS, Ha JH, Paeng JC, Han I. Total lesion glycolysis by 18F-FDG PET/CT is a reliable predictor of prognosis in soft-tissue sarcoma. Eur J Nucl Med Mol Imaging. 2013;40(12):1836–42.

12. Im H-J, Kim YK, Kim Y-i, Lee JJ, Lee WW, Kim SE. Usefulness of combined metabolic–volumetric indices of 18F-FDG PET/CT for the early prediction of neoadjuvant chemotherapy outcomes in breast cancer. Nucl Med and Mole Imaging. 2013:1-8.

13. Hatt M, Visvikis D, Albarghach NM, Tixier F, Pradier O, Cheze-le RC. Prognostic value of 18F-FDG PET image-based parameters in oesophageal cancer and impact of tumour delineation methodology. Eur J Nucl Med Mol Imaging. 2011;38(7):1191–202.

14. Holli K, Laaperi AL, Harrison L, Luukkaala T, Toivonen T, Ryymin P, et al. Characterization of breast cancer types by texture analysis of magnetic resonance images. Acad Radiol. 2010;17(2):135–41.

15. Davnall F, Yip CS, Ljungqvist G, Selmi M, Ng F, Sanghera B, et al. Assessment of tumor heterogeneity: an emerging imaging tool for clinical practice? Insights Imaging. 2012;3(6):573–89.

16. Ba-Ssalamah A, Muin D, Schernthaner R, Kulinna-Cosentini C, Bastati N, Stift J, et al. Texture-based classification of different gastric tumors at contrast-enhanced CT. Eur J Radiol. 2013;82(10):e537–43.

17. Cook GJ, Yip C, Siddique M, Goh V, Chicklore S, Roy A, et al. Are pretreatment 18F-FDG PET tumor textural features in non–small cell lung cancer associated with response and survival after chemoradiotherapy? J Nucl Med. 2013;54(1):19–26.

18. Maemondo M, Inoue A, Kobayashi K, Sugawara S, Oizumi S, Isobe H, et al. Gefitinib or chemotherapy for non-small-cell lung cancer with mutated EGFR. N Engl J Med. 2010;362(25):2380–8.

19. Vesselle H, Salskov A, Turcotte E, Wiens L, Schmidt R, Jordan CD, et al. Relationship between non-small cell lung cancer FDG uptake at PET, tumor histology, and Ki-67 proliferation index. J Thorac Oncol. 2008;3(9):971–8.

20. Choi H, Paeng JC, Kim D-W, Lee JK, Park CM, Kang KW, et al. Metabolic and metastatic characteristics of ALK-rearranged lung adenocarcinoma on FDG PET/CT. Lung Cancer. 2012;79(3):242-7.

21. Putora PM, Fruh M, Muller J. FDG-PET SUV-max values do not correlate with epidermal growth factor receptor mutation status in lung adenocarcinoma. Respirology. 2013;18(4):734–5.

22. Cheng NM, Fang YH, Yen TC. The promise and limits of PET texture analysis. Ann Nucl Med. 2013;27(9):867–9.

23. Wu H, Sun T, Wang J, Li X, Wang W, Huo D, et al. Combination of radiological and gray level co-occurrence matrix textural features used to distinguish solitary pulmonary nodules by computed tomography. J Digit Imaging. 2013;26(4):797–802.

24. Chicklore S, Goh V, Siddique M, Roy A, Marsden PK, Cook GJ. Quantifying tumour heterogeneity in 18F-FDG PET/CT imaging by texture analysis. Eur J Nucl Med Mol Imaging. 2013;40(1):133–40.

25. Ye J, Janardan R, Li Q. Two-dimensional linear discriminant analysis. In: Advances in neural information processing systems. San Mateo: Morgan Kaufmann Publishers; 2004.

26. Larson SM. Cancer or inflammation? A holy grail for nuclear medicine. J Nucl Med. 1994;35(10):1653–5.

27. Buck AK, Halter G, Schirrmeister H, Kotzerke J, Wurziger I, Glatting G, et al. Imaging proliferation in lung tumors with PET: 18F-FLT versus 18F-FDG. J Nucl Med. 2003;44(9):1426–31.

28. Galavis PE, Hollensen C, Jallow N, Paliwal B, Jeraj R. Variability of textural features in FDG PET images due to different acquisition modes and reconstruction parameters. Acta Oncol. 2010;49(7):1012–6.